Supplementary Information: Energy-resolved and time-dependent unimolecular dissociation of hydroperoxyalkyl radicals (•QOOH)

Trisha Bhagde[1*], Anne S. Hansen[1*], Shuguang Chen[1], Patrick J. Walsh[1], Stephen J. Klippenstein[2], and Marsha I. Lester[1]

[1] Department of Chemistry, University of Pennsylvania, Philadelphia, PA 19104-6323, USA
[2] Chemical Sciences and Engineering Division, Argonne National Laboratory, Lemont, IL 60439, USA

Table of Contents

S1. Methods

S1.1. Deuteration of the TBHP hydroperoxyl group

A commercial sample of *tert*-butyl hydroperoxide ($(CH_3)_3COOH$, ACROS Organics, 70% TBHP aqueous solution) is dried using the procedure described previously.[1, 2] The dried sample of 5mL TBHP in a 100 mL round bottom flask is dissolved in 30 mL methylene chloride (DCM Stabilized/Certified ACS, Fisher Chemical). Next, 10 ml of D_2O (deuterium oxide, D 99.9%, Cambridge Isotope Laboratories) is added with continuous stirring for 20 minutes. This mixture is transferred to a 250 mL separatory funnel. Once the aqueous layer (D_2O) and DCM layer separate, the DCM layer is collected in a round bottom flask. The DCM layer is then resubjected to the deuteration procedure 8–9 times with fresh 10 mL charges of D_2O. Once the desired amount of deuteration is achieved, as judged by ^{1}H NMR integration of the residual O–H peak against the *tert*-butyl group in $CDCl_3$, the DCM layer is dried over anhydrous $MgSO_4$ for 1 h. The DCM layer is filtered into a round bottom flask and concentrated under reduced pressure for 20 min at room temperature. To further reduce the residual DCM in the final peroxide product, the flask is attached to a vacuum line for ~ 2 h. After this period, approximately 2 mL colorless liquid *tert*-BuOOD is recovered. Note that care must be used when removing the residual CH_2Cl_2 in order to not evaporate all the desired peroxide product. ^{1}H NMR integration of the *tert*-butyl group against the residual OH (Figure S1) gave a ratio of approximately 134:1 (Figure S2), indicating a percentage deuteration of ca. 93% at the hydroperoxy moiety.

S1.2. Experimental

A carrier gas composed of 0.25% Cl_2 (Airgas), 25% He, and 75% Ar (Praxair) at a pressure of 40 psi is used to entrain the vapor of dried and deuterated $(CH_3)_3COOD$ (TBDP). Due to the presence of corrosive Cl_2, the sample line is constructed using Hastealloy (McMaster Carr) and Teflon tubing. A solenoid valve (Parker General Valve Series 9) with an affixed quartz capillary reactor tube (~25 mm length and 1 mm ID) pulses the gas mixture into a vacuum chamber. Cl atoms are generated by photolyzing Cl_2 along the length of the capillary tube using the cylindrically focused third harmonic output of a Nd:YAG laser (Continuum Powerlite Precision 8000, 355 nm, ~5 mJ/pulse, 10 Hz). The photolytically generated Cl atoms can abstract one of the nine H-atoms associated with the three methyl groups of TBDP.[3] This results in the formation of the partially deuterated 2-deuteroperoxy-2-methylprop-1-yl ($\bullet CH_2(CH_3)_2COOD$ or •QOOD) and HCl products as shown in Scheme S1. The resultant •QOOD along with the other components of the carrier gas mixture subsequently undergo a supersonic jet expansion resulting in collisional stabilization and cooling of •QOOD to a rotational temperature of ca. 10 K.[4, 5]

Approximately 1 cm downstream, the gas mixture is intersected by counter-propagating and spatially overlapped IR-pump and UV-probe laser beams focused to ca. 3 and 5 mm diameters, respectively. A KDP crystal (Inrad) is used to frequency double the output of an Nd:YAG (Continuum 7020; 532 nm, 10 Hz) pumped dye laser (ND6000, Rhodamine 590 and 610 dye) to obtain the UV probe beam (~3 mJ/pulse, ~6 ns FWHM). The signal output of an optical parametric oscillator/amplifier (OPO/OPA, Laservision; 0.9 cm^{-1} bandwidth) pumped by a Nd:YAG laser (1064 nm, Continuum Surelite EX, 5 Hz) is the tunable IR pump beam (~30 mJ/pulse, ~6 ns FWHM). IR activation of •QOOD generates OD $X^2\Pi_{3/2}$ (v=0) products as shown in Scheme S2. UV laser-induced fluorescence (LIF) on the OD $A^2\Sigma^+ – X^2\Pi_{3/2}$ (1,0) $Q_1(3.5)$ transition is used to probe the resultant OD products.

IR action spectra of •QOOD are obtained by introducing the IR pump beam 50 – 100 ns prior to the UV probe beam and scanning the IR wavelength. Lifetime measurements are carried out with fixed IR excitation while the time delay between the IR pump and UV probe is scanned using a digital delay generator (BNC model 565). The OD $A^2\Sigma^+ – X^2\Pi_{3/2}$ (1,1) fluorescence is collected using f/1 optics, which is passed through a 313 nm bandpass filter (OD 4, Edmund Optics) and detected with a gated photomultiplier tube (Electron Tubes 9813QB PMT). The LIF signal is preamplified and displayed on an oscilloscope (LeCroy WaveRunner 44Xi) interfaced with a computer for processing. Background OD LIF signal, not induced by IR excitation, is removed by an active background subtraction scheme (IR on – IR off).[6] Additional details about the experimental setup are given in Refs. 7-9.

The overall temporal profile is fitted with a dual exponential function, $F(t)$:

$$F(t) = A\exp\left(-k_{\text{fall}}t + \frac{1}{4}\,k_{\text{fall}}^2\left(\Delta t_{\text{IR}}^2 + \Delta t_{\text{UV}}^2\right)\right) - B\exp\left(-(k_{\text{fall}} + k_{\text{rise}})t + \frac{1}{4}(k_{\text{fall}} + k_{\text{rise}})^2\left(\Delta t_{\text{IR}}^2 + \Delta t_{\text{UV}}^2\right)\right) \quad \text{(S1)}$$

Here, A and B are amplitudes of the fit, k_{rise} and k_{fall} are the rise and fall in OD LIF intensity, and Δt_{IR} (2.8 ± 0.1 ns) and Δt_{UV} (3.0 ± 0.1 ns) are the IR and UV temporal pulse widths (Gaussian), respectively. This yields a time resolution of Δt = 4.1 ± 0.1 ns and corresponds to a full width at half maximum (FWHM) of 6.9 ± 0.1 ns. The experimental rate for appearance of OD products is determined to be $k_{\text{rise}} = 1.0 \pm 0.3 \times 10^8$ s^{-1}, corresponding to a risetime of 9.8 ± 3.0 ns, with uncertainty (±1σ) derived from repeated measurements. k_{rise} is insensitive to the ca. 150 times slower k_{fall} ($k_{\text{fall}} = 6.9 \pm 0.3 \times 10^5$ s^{-1}; τ_{fall} = 1450 ± 50 ns based on typical measurements).[9]

S2. Schemes

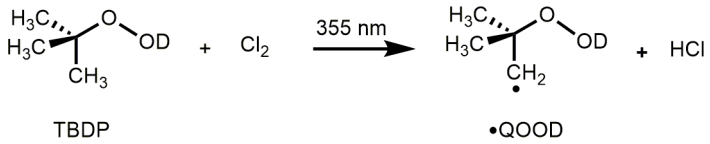

Scheme S1: Chlorine radicals generated by 355 nm photolysis of Cl_2 abstract a hydrogen atom from one of the methyl groups of TBDP resulting in the formation of •QOOD and HCl.

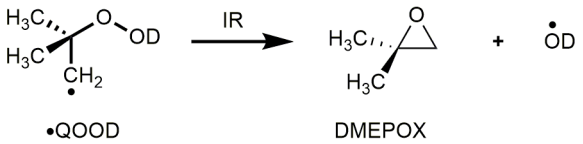

Scheme S2: IR excitation of •QOOD on the overtone OD stretch results in unimolecular decay to 2,2-dimethyl epoxide (DMEPOX) and OD products, the latter of which is detected by LIF.

S3. Figures

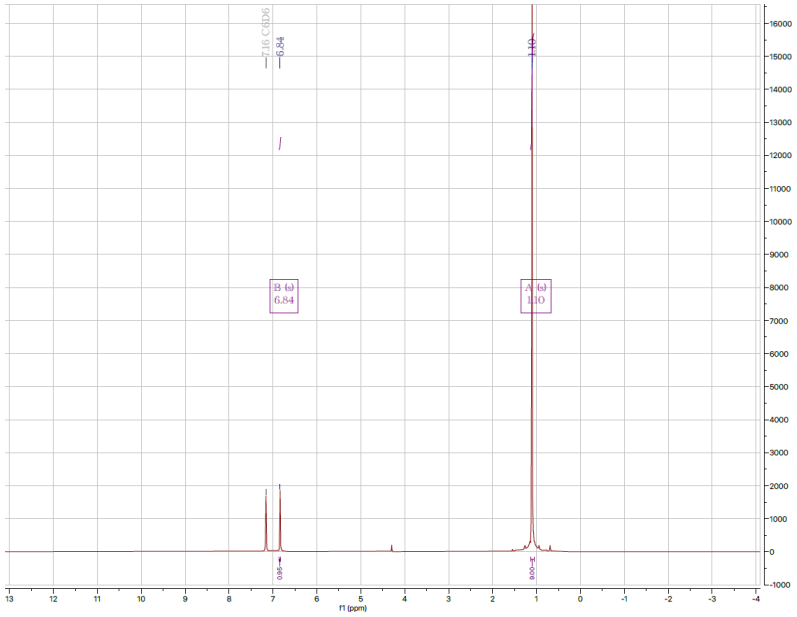

Figure S1: 1H NMR of dried TBHP in C_6D_6 showing a ratio of protons from the methyl to the hydroperoxy group as 9:1.

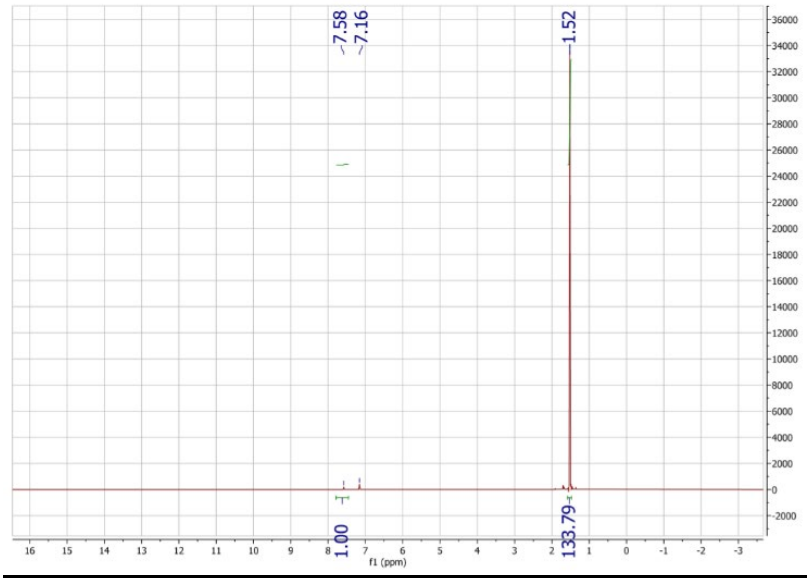

Figure S2: ^{1}H NMR of TBDP in C_6D_6 showing a ratio of protons from the methyl to the hydroperoxy group as 134:1, indicating partial deuteration of 93% of the H atom at the hydroperoxy site.

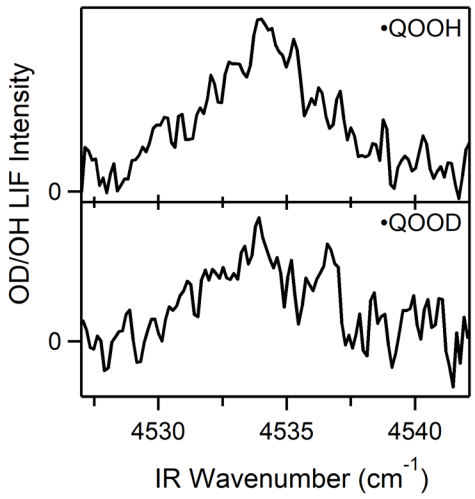

Figure S3: Experimental IR action spectra of the $\nu_{CH_2} + \delta_{CH_2}$ transition peaking at 4534.0 cm^{-1} for both •QOOH and •QOOD with OH and OD LIF detection, respectively, recorded at a 100 ns time delay between the IR pump and UV probe lasers.[10] Both the computed and observed $\nu_{CH_2} + \delta_{CH_2}$ transitions are unchanged (Table 1) upon deuteration of the hydroperoxy (OOH/D) group. The intensities are in arbitrary units, although the signal level achieved for •QOOD is weaker.

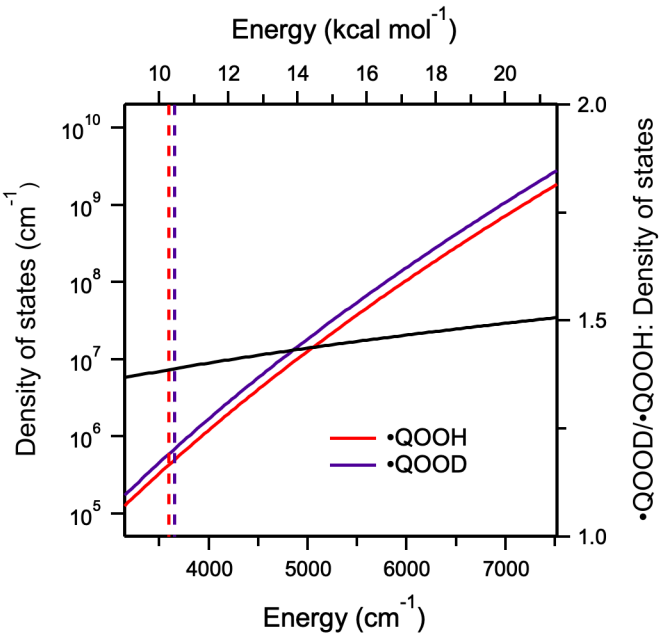

Figure S4: The density of states for •QOOH (red) and •QOOD (purple) used to determine the RRKM dissociation rates in Figure 5, along with the ratio of the •QOOD to •QOOH density of states (black). The increase in density of states for •QOOD results from the frequency changes that occur upon deuteration. The vertical dashed lines indicate the slightly higher transition state (TS) barrier for •QOOD (10.5 kcal mol^{-1}, purple) compared to that for •QOOH (10.3 kcal mol^{-1}, red).

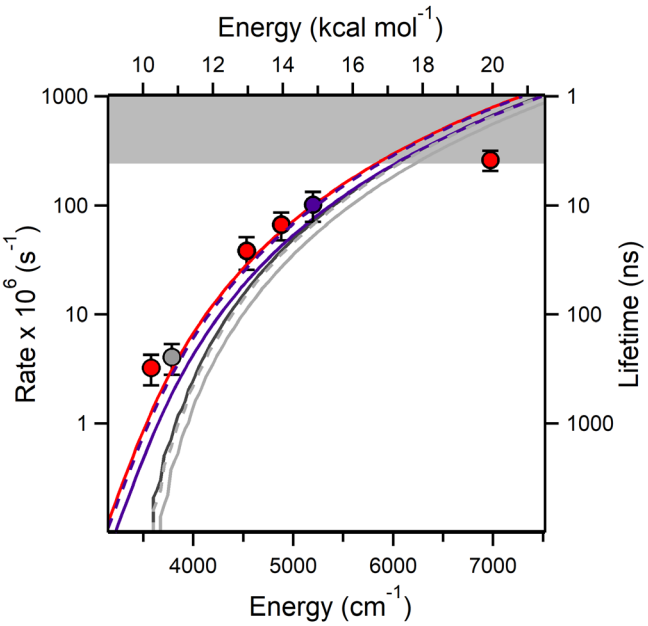

Figure S5: Rates and lifetimes (semi-log scale) for the unimolecular decay reactions of •QOOD and •QOOH reproduced from Figure 5 in main text. The experimental rates are given by the circles (•QOOD in purple and •QOOH in red and gray) with error bars (±1σ) derived from repeated measurements. RRKM rates and lifetimes are calculated with tunneling (solid lines, •QOOD in purple and •QOOH in red) and without tunneling (solid lines, •QOOD in light gray and •QOOH in dark gray). The additional dashed lines are decay rates predicted for •QOOD with the TS barrier artificially set at 10.3 kcal mol^{-1}, the same as that for •QOOH, with (purple) and without (gray) tunneling. The gray shaded region indicates rates limited by the experimental time resolution (4 ns).

Table S1: Calculated fundamental harmonic and anharmonic frequencies and intensities of •QOOD using different methods.

Number	Harmonic			Anharmonic		
	CCSD(T)[a] Frequency (cm^{-1})	B2PLYP-D3[b] Frequency (cm^{-1})	B2PLYP-D3[b] Intensity (km mol^{-1})	CCSD(T)[c] Frequency (cm^{-1})	B2PLYP-D3[b] Frequency (cm^{-1})	B2PLYP-D3[b] Intensity (km mol^{-1})[d]
1	3259	3278	7.36	3118	3137	7.78
2	3145	3165	9.83	3028	3049	19.5
3	3141	3154	12.5	3006	3019	14.7
4	3132	3144	19.1	3012	3024	16.4
5	3128	3141	21.8	2988	3000	19.6
6	3122	3134	7.10	2990	3002	8.60
7	3047	3064	13.8	2934	2951	11.5
8	3044	3060	14.0	2946	2962	2.46
9	2754	2751	16..0	2650	2647	11.9
10	1520	1524	5.97	1479	1484	0.97
11	1502	1506	2.71	1463	1467	1.45
12	1495	1500	0.57	1458	1463	0.68
13	1486	1490	2.19	1445	1449	3.13
14	1469	1474	4.63	1430	1435	4.20
15	1416	1418	12.0	1382	1384	8.71
16	1403	1402	13.1	1370	1370	11.3
17	1293	1291	15.8	1254	1253	10.8
18	1289	1280	9.27	1235	1226	4.60
19	1172	1167	32.6	1150	1145	19.9
20	1041	1043	1.83	1024	1026	1.57
21	1019	1016	24.9	1011	1008	9.99
22	996	994	0.71	956	955	1.08
23	957	962	0.47	973	978	2.29
24	929	930	1.56	897	898	1.36
25	910	914	6.96	874	878	6.30
26	861	848	15.4	836	823	7.53
27	775	773	4.00	760	757	4.85
28	592	596	29.6	658	662	18.6
29	496	498	2.43	506	507	0.56
30	445	451	8.12	428	434	
31	394	402	2.98	386	394	
32	351	354	3.89	358	360	
33	328	329	5.89	322	324	
34	256	256	6.07	263	263	
35	253	253	0.26	246	245	
36	215	210	0.58	82	78	
37	179	182	55.4	33	37	
38	141	140	5.27	191	190	
39	117	105	6.36	181	170	

a. Obtained with the CCSD(T)-F12/cc-pVDZ-F12 level of theory.
b. Obtained with the B2PLYP-D3/cc-pVTZ level of theory.
c. Obtained combining the harmonic frequencies from the CCSD(T)-F12/cc-pVDZ-F12 method with the anharmonic corrections from the B2PLYP-D3/cc-pVTZ method, and used for the RRKM calculations.
d. Computed intensities for low frequency anharmonic vibrations (<500 cm^{-1}) are not included.

Table S2: Calculated anharmonic frequency and intensity (VPT2) of the overtone OD stretch ($2\nu_{OD}$) for •QOOD conformers (•QOOD1, •QOOD2, and •QOOD3) and TBDP using the B2PLYP-D3/cc-pVTZ level of theory.

Species	Frequency (cm^{-1})	Intensity (km mol^{-1})
•QOOD1	5200.7	2.0
•QOOD2	5218.7	2.1
•QOOD3	5224.1	2.1
TBDP	5228.9	2.0

Table S3: Calculated contributions to the harmonic zero-point energy (ZPE) correction for the reactants (•QOOH and •QOOD), the corresponding transition state barriers (TS), and change in ZPE (ΔZPE). The resulting transition state barriers leading to OH/OD + cyclic ether products are also given.

•QOOH (kcal mol^{-1})			
ZPE harmonic		ΔZPE	Barrier
•QOOH	TS		
77.95	76.77	1.18	10.28[a]

•QOOD (kcal mol^{-1})			
ZPE harmonic		ΔZPE	Barrier
•QOOD	TS		
75.87	74.86	1.01	10.45

a: Ref. 9.

Table S4: Calculated RRKM unimolecular microcanonical rates ($k(E)$, corresponds to k_{rise}) and corresponding lifetimes (τ) calculated for unimolecular decay of •QOOD and •QOOH with tunneling.

	•QOOD		•QOOH	
Energy	$k(E)$	τ	$k(E)$	τ
(cm^{-1})	(s^{-1})	(ns)	(s^{-1})	(ns)
2800	9.13×10^{3}	110×10^{3}	1.71×10^{4}	583×10^{2}
2900	1.62×10^{4}	618×10^{2}	3.04×10^{4}	329×10^{2}
3000	2.88×10^{4}	348×10^{2}	5.39×10^{4}	185×10^{2}
3100	5.11×10^{4}	196×10^{2}	9.55×10^{4}	105×10^{2}
3200	9.05×10^{4}	111×10^{2}	1.69×10^{5}	5930
3300	1.59×10^{5}	6270	2.96×10^{5}	3380
3400	2.78×10^{5}	3590	5.12×10^{5}	1950
3500	4.78×10^{5}	2090	8.64×10^{5}	1160
3600	7.99×10^{5}	1250	1.41×10^{6}	711
3700	1.29×10^{6}	777	2.20×10^{6}	455
3800	1.99×10^{6}	502	3.30×10^{6}	303
3900	2.97×10^{6}	336	4.79×10^{6}	209
4000	4.29×10^{6}	233	6.75×10^{6}	148
4100	6.01×10^{6}	166	9.24×10^{6}	108
4200	8.21×10^{6}	122	1.24×10^{7}	80.5
4300	1.09×10^{7}	91.4	1.62×10^{7}	61.6
4400	1.43×10^{7}	69.7	2.09×10^{7}	47.9
4500	1.85×10^{7}	54.1	2.65×10^{7}	37.7
4600	2.35×10^{7}	42.6	3.31×10^{7}	30.2
4700	2.93×10^{7}	34.1	4.08×10^{7}	24.5
4800	3.62×10^{7}	27.6	4.99×10^{7}	20.1
4900	4.42×10^{7}	22.6	6.02×10^{7}	16.6
5000	5.34×10^{7}	18.7	7.19×10^{7}	13.9
5100	6.39×10^{7}	15.7	8.53×10^{7}	11.7
5200	7.59×10^{7}	13.2	1.00×10^{8}	9.97
5300	8.94×10^{7}	11.2	1.17×10^{8}	8.52
5400	1.04×10^{8}	9.58	1.36×10^{8}	7.35
5500	1.22×10^{8}	8.23	1.57×10^{8}	6.36
5600	1.40×10^{8}	7.15	1.80×10^{8}	5.55
5700	1.61×10^{8}	6.22	2.05×10^{8}	4.88
5800	1.84×10^{8}	5.45	2.34×10^{8}	4.28
5900	2.09×10^{8}	4.78	2.64×10^{8}	3.79
6000	2.36×10^{8}	4.23	2.97×10^{8}	3.37
6100	2.66×10^{8}	3.75	3.33×10^{8}	3.01
6200	2.99×10^{8}	3.34	3.71×10^{8}	2.69
6300	3.35×10^{8}	2.99	4.13×10^{8}	2.42
6400	3.73×10^{8}	2.68	4.58×10^{8}	2.18
6500	4.14×10^{8}	2.42	5.06×10^{8}	1.98
6600	4.58×10^{8}	2.18	5.58×10^{8}	1.79
6700	5.05×10^{8}	1.98	6.13×10^{8}	1.63
6800	5.56×10^{8}	1.80	6.71×10^{8}	1.49
6900	6.10×10^{8}	1.64	7.34×10^{8}	1.36

7000	6.67×10^8	1.50	8.01×10^8	1.25
7100	7.28×10^8	1.37	8.71×10^8	1.15
7200	7.93×10^8	1.26	9.46×10^8	1.06
7300	8.61×10^8	1.16	1.02×10^9	0.98
7400	9.34×10^8	1.07	1.11×10^9	0.90
7500	1.01×10^9	0.99	1.19×10^9	0.84
7600	1.09×10^9	0.92	1.29×10^9	0.77
7700	1.17×10^9	0.85	1.39×10^9	0.72
7800	1.27×10^9	0.79	1.48×10^9	0.67
7900	1.36×10^9	0.74	1.59×10^9	0.63
8000	1.46×10^9	0.69	1.70×10^9	0.59
8100	1.56×10^9	0.64	1.82×10^9	0.55
8200	1.67×10^9	0.60	1.94×10^9	0.52
8300	1.78×10^9	0.56	2.06×10^9	0.48
8400	1.90×10^9	0.53	2.20×10^9	0.45
8500	2.02×10^9	0.49	2.33×10^9	0.43
8600	2.15×10^9	0.47	2.48×10^9	0.40
8700	2.28×10^9	0.44	2.62×10^9	0.38

References

1. A. S. Hansen, R. M. Huchmala, E. Vogt, M. A. Boyer, T. Bhagde, M. F. Vansco, C. V. Jensen, A. Kjærsgaard, H. G. Kjaergaard, A. B. McCoy and M. I. Lester, *J. Chem. Phys.*, 2021, **154**, 164306.
2. J. Sharpless and T. R. Verhoeven, *Aldrichimica Acta.*, 1979, **12**, 63-74.
3. S. J. Blanksby and G. B. Ellison, *Acc. Chem. Res.*, 2003, **36**, 255-263.
4. F. Liu, J. M. Beames, A. S. Petit, A. B. McCoy and M. I. Lester, *Science*, 2014, **345**, 1596-1598.
5. F. Liu, J. M. Beames and M. I. Lester, *J. Chem. Phys.*, 2014, **141**, 234312.
6. S. Hsieh, R. Vushe, Y. T. Tun and J. L. Vallejo, *Chem. Phys. Lett.*, 2014, **591**, 99-102.
7. Y. Fang, F. Liu, V. P. Barber, S. J. Klippenstein, A. B. McCoy and M. I. Lester, *J. Chem. Phys.*, 2016, **144**, 061102.
8. V. P. Barber, S. Pandit, A. M. Green, N. Trongsiriwat, P. J. Walsh, S. J. Klippenstein and M. I. Lester, *J. Am. Chem. Soc.*, 2018, **140**, 10866-10880.
9. A. S. Hansen, T. Bhagde, K. B. Moore, D. R. Moberg, A. W. Jasper, Y. Georgievskii, M. F. Vansco, S. J. Klippenstein and M. I. Lester, *Science*, 2021, **373**, 679-682.
10. A. S. Hansen, T. Bhagde, Y. Qian, A. Cavazos, R. M. Huchmala, M. A. Boyer, C. F. Gavin-Hanner, S. J. Klippenstein, A. B. McCoy and M. I. Lester, *J. Chem. Phys.*, 2022, **156**, 014301.